

Article

A Novel Parameter Estimation Method Based on Piecewise Nonlinear Amplitude Transform for the LFM Signal in Impulsive Noise

Haiying Wang ^{1,2,3} , Qunying Zhang ^{1,2,*}, Wenhai Cheng ^{1,2,3} , Jiaming Dong ^{1,2,3}  and Xiaojun Liu ^{1,2}

¹ Aerospace Information Research Institute, Chinese Academy of Sciences, Beijing 100190, China; wanghaiying20@mails.ucas.ac.cn (H.W.)

² Key Laboratory of Electromagnetic Radiation and Sensing Technology, Chinese Academy of Sciences, Beijing 100190, China

³ School of Electronic, Electrical and Communication Engineering, University of Chinese Academy of Sciences, Beijing 100190, China

* Correspondence: qyzhang@mail.ie.ac.cn; Tel.: +86-13311572815

Abstract: In a complex electromagnetic environment, any noise present generally exhibits strong impulsive characteristics. The performance of existing parameter estimation methods carried out in Gaussian white noise for the linear frequency modulation (LFM) signal degrades or even fails under impulsive noise. This paper proposes a novel parameter estimation method to address this problem. Firstly, the properties of the piecewise nonlinear amplitude transform (PNAT) are derived. This manuscript verifies that the PNAT can retain phase information of the LFM signal while suppressing the impulsive noise. Subsequently, a new concept known as piecewise nonlinear amplitude transform parametric symmetric instantaneous autocorrelation function (PNAT-PSIAF) is proposed. Based on this concept, a novel method called piecewise nonlinear amplitude transform Lv's distribution (PNAT-LVD) is proposed to estimate the centroid frequency and chirp rate of the LFM signal. The simulations show that the proposed algorithm can effectively suppress the impulsive noise without prior knowledge of the noise for both the single-component and double-component LFM signal. In addition, two parameters of the LFM signal can be precisely estimated by the proposed method under low generalized signal-to-noise ratios (GSNR). The stronger the impulsive characteristics of the noise, the better the performance of the algorithm.

Keywords: parameter estimation; the LFM signal; piecewise nonlinear amplitude transform; Lv's distribution; impulsive noise



Citation: Wang, H.; Zhang, Q.; Cheng, W.; Dong, J.; Liu, X. A Novel Parameter Estimation Method Based on Piecewise Nonlinear Amplitude Transform for the LFM Signal in Impulsive Noise. *Electronics* **2023**, *12*, 2530. <https://doi.org/10.3390/electronics12112530>

Academic Editors: Yin Zhang, Deqing Mao, Yulin Huang and Yachao Li

Received: 30 April 2023

Revised: 30 May 2023

Accepted: 31 May 2023

Published: 3 June 2023



Copyright: © 2023 by the authors. Licensee MDPI, Basel, Switzerland. This article is an open access article distributed under the terms and conditions of the Creative Commons Attribution (CC BY) license (<https://creativecommons.org/licenses/by/4.0/>).

1. Introduction

The LFM signal is frequently utilized in sonar, communication, biomedical, and radar applications [1–5]. As a non-stationary signal with strong low probability of intercept (LPI) characteristics, the LFM signal is frequently used in radars of different systems. In radar countermeasures, accurate parameter estimation is critical for subsequent radar jamming, radar electronic defense, and adjustment of combat strategies. The centroid frequency and the chirp rate are two significant parameters characterizing the LFM signal.

Many methods have been proposed to estimate the LFM signal's parameters, such as maximum likelihood estimator (MLE) [6–8] and time-frequency (TF) analysis methods [9–17]. Among the proposed methods, MLE exhibits the best estimation of the parameters theoretically, and its performance approximates the Cramer-Rao Lower Bound (CRLB). Nevertheless, the parameter estimation process of MLE requires a multi-dimensional search, which requires extensive computational resources and is not conducive to engineering implementation. When processing non-stationary signals, particularly when estimating the parameters of the LFM signal, the T-F analysis method is quite effective. The short-time

Fourier transform (STFT) [9,10] is the earliest time-frequency analysis method. The T-F distribution established by this method is simple and intuitive, but the time-frequency resolution of this method cannot be flexibly changed when analyzing non-stationary signals. The Wigner–Ville distribution (WVD) [11–13] achieves the highest energy accumulation in the TF plane. To achieve parameter estimation of the LFM signal, the WVD is usually combined with the Hough transform to form Wigner-Hough transform (WHT). However, this method will produce serious cross-term interference when processing the multi-component LFM signal, and is also computationally intensive. The Fractional Fourier transform (FRFT) [14–17] is extended from the traditional Fourier transform, and it obtains a new FRFT domain by rotating the signal in the TF plane. The signal's energy will accumulate to form a peak in the FRFT domain once the rotation angle is suitable. Parameter estimation of the signal can be achieved by searching for the peak. Nevertheless, this method requires a two-dimensional search, and the computational demand is relatively great when high accuracy is required for parameter estimation.

Most of the above parameter estimation methods are carried out in the environment of Gaussian white noise. However, in real-world electromagnetic environments, hydroacoustic noise, atmospheric noise, and radar clutter are non-Gaussian noise. These types of noise exhibit prominent impulsive characteristics and can be described as impulsive noise. The performance of all the parameter estimation methods mentioned above will experience significant degradation in conditions of strong impulsive noise. To solve this problem, the authors in [18] combined the concept of fractional low-order (FLO) covariance with WHT and Lv's distribution (LVD) [19] and proposed the methods of FLO-WHT and FLO-LVD. Although the methods concerned with fractional low-order can effectively suppress the impulse noise, the methods require specific prior information of the noise. Moreover, the performance of the methods degrades rapidly when the order of fractional low-order methods is not appropriate. In the work of [20,21], a parameter estimation method based on the Sigmoid function and FRFT (Sigmoid-FRFT) is proposed, which does not require a priori information of the noise and suppresses the impulsive noise well. However, this method may fail when processing the plural signal. In general, the existing methods used to suppress impulsive noise face the following problems: (1) a priori knowledge of the noise is required; (2) they may fail when processing complex signals; and (3) the suppression capability of strong impulsive noise is limited.

To solve these problems, a new parameter estimation method known as PNAT-LVD is proposed in this manuscript. First, the properties of the PNAT are derived to confirm that the phase information of the LFM signal remains unchanged after PNAT while suppressing the impulsive noise. The parametric symmetric instantaneous autocorrelation function (PSIAF) [22] of the signal after PNAT is then calculated to obtain the PNAT-PSIAF. Next, the PNAT-PSIAF is scaled-transformed to achieve the decoupling relationship between time and delay. Finally, a two-dimensional Fourier transform is performed to obtain the PNAT-LVD. By searching for the peak coordinates of the PNAT-LVD, the centroid frequency and the chirp rate of the LFM signal can be estimated. The simulations show that the proposed algorithm can successfully reduce the influence of impulsive noise and does not require knowledge of the noise beforehand. Meanwhile, the two parameters can still be precisely estimated under strong impulsive noise.

The remainder of this paper is structured as follows. In Section 2, the models of the signal and noise are developed. In Section 3, the Lv's distribution algorithm is introduced, and the shortcomings of this algorithm under impulsive noise are analyzed. In Section 4, an improved algorithm known as PNAT-LVD is proposed, and two important properties of PNAT are proposed and proved. Furthermore, the optimal scale parameter used in PNAT-LVD is discussed. In Section 5, several sets of simulations are conducted to confirm the efficacy of the proposed method. Lastly, concluding remarks are provided in Section 6.

2. The Models of the Signal and the Impulsive Noise

2.1. The LFM Signal Model

Typically, a continuous multi-component LFM signal is defined as follows [23]:

$$x(t) = \sum_{i=1}^l A_i \exp \left[j2\pi \left(f_{0i}t + \frac{1}{2}k_i t^2 \right) \right] \quad -\frac{T}{2} \leq t \leq \frac{T}{2} \quad (1)$$

where l is the number of signal components, when l equals 1, $x(t)$ depicts the single-component LFM signal. A_i depicts the amplitude of the i th signal component, f_{0i} depicts the centroid frequency of the i th signal component, k_i depicts the chirp rate of the i th signal component, and T depicts the signal's pulse width. Assume that the LFM signal in the impulsive noise is $s(t)$, then

$$s(t) = x(t) + n(t) \quad (2)$$

where $x(t)$ is the LFM signal and $n(t)$ is the impulsive noise.

2.2. The Impulsive Noise Model

For noise with strong randomness and impulsiveness in complex electromagnetic environments, the symmetric α -stable ($S\alpha S$) distribution noise model can be used to describe accurately [24,25]. Therefore, the impulsive noise model used in this paper is the $S\alpha S$ distribution noise model. Since the probability density function (PDF) of the random variable that obeys the $S\alpha S$ distribution does not have a closed form, the characteristic function is generally used to represent [26]:

$$\varphi(t) = \exp jbt - \gamma |t|^\alpha [1 + j\beta \operatorname{sgn}(t)w(t, \alpha)] \quad (3)$$

where

$$w(t, \alpha) = \begin{cases} \frac{2}{\pi} \lg |t| & \alpha = 1 \\ \tan \frac{\alpha\pi}{2} & \alpha \neq 1 \end{cases} \quad (4)$$

$$\operatorname{sgn}(t) = \begin{cases} 1, & t > 0 \\ 0, & t = 0 \\ -1, & t < 0 \end{cases} \quad (5)$$

where $\operatorname{sgn}(t)$ is a symbolic function, $b(-\infty < b < +\infty)$ is the location parameter that reflects the location of the center of the distribution. $\alpha(0 < \alpha \leq 2)$ is a characteristic index reflecting the strength of noise impulsivity. The smaller its value, the stronger the noise impulsivity. $\beta(-1 \leq \beta \leq 1)$ is a symmetric parameter. When $\beta = 0$, the noise obeys $S\alpha S$ distribution. $\gamma(\gamma > 0)$ is a scale parameter that measures the degree of the sample's departure from the mean. Since there is no finite second-order moment of the $S\alpha S$ distribution noise, the conventional signal-to-noise ratio (SNR) is no longer applicable. Therefore, the GSNR [27] is used to describe the relationship between the signal and the $S\alpha S$ distribution noise.

$$\text{GSNR} = 10 \lg \left(\frac{\sigma_s^2}{\gamma} \right) \quad (6)$$

where σ_s^2 depicts the signal's variance, and γ depicts the noise's scale parameter mentioned before [28].

3. The Lv's Distribution Algorithm

The LVD is a relatively time-frequency analysis method applied to estimate the chirp rate and the centroid frequency of the LFM signal. Compared with WVD, this method can estimate parameters without relying on linear detection methods such as the Hough transform and has higher energy accumulation. Meanwhile, the Lv's distribution also performs better than FRFT in resolution, representation, and detection. Therefore, the Lv's

distribution has an essential advantage in the parameter estimation of the LFM signal. Take the signal with the form of (1) as an example. Define the PSIAF of the signal as follows [19]:

$$\begin{aligned}
 R_x(t, \tau) &= x\left(t + \frac{\tau + a}{2}\right) x^*\left(t - \frac{\tau + a}{2}\right) \\
 &= \sum_{i=1}^l R_{x_i}(t, \tau) + \sum_{i=1}^{l-1} \sum_{j=i+1}^l \left[R_{x_i x_j}(t, \tau) + R_{x_j x_i}(t, \tau) \right] \\
 &= \sum_{i=1}^l A_i^2 \exp[j2\pi f_{0i}(\tau + a) + j2\pi k_i(\tau + a)t] \\
 &\quad + \sum_{i=1}^{l-1} \sum_{j=i+1}^l \left[R_{x_i x_j}(t, \tau) + R_{x_j x_i}(t, \tau) \right]
 \end{aligned} \tag{7}$$

where * denotes complex conjugation, τ denotes the time delay, R_{s_i} denotes the auto-term, $R_{s_i s_j}$ denotes the cross-term, and a is the delay constant concerned with a scaling operator whose optimal value is generally taken as 1. In order to uncouple the time variable t and the time delay τ , a scale transformation of the time variable t is required, as shown in the following equation.

$$\Gamma[R(t, \tau)] = R\left(\frac{t_n}{h(\tau + a)}, \tau\right) \tag{8}$$

where h is a scale operator, the best performance of the scale transformation is achieved when h equals 1 [19]. A scale transformation of Equation (7) then gives

$$\begin{aligned}
 \Gamma[R_x(t, \tau)] &= \sum_{i=1}^l A_i^2 \exp\left[j2\pi f_{0i}(\tau + a) + j2\pi \frac{k_i}{h} t_n\right] \\
 &\quad + \sum_{i=1}^{l-1} \sum_{j=i+1}^l \left[R_{x_i x_j}(t_n, \tau) + R_{x_j x_i}(t_n, \tau) \right]
 \end{aligned} \tag{9}$$

The expression of LVD is obtained by making a two-dimensional Fourier transformation of t_n and τ based on Equation (9).

$$\begin{aligned}
 LVD_x(f, k) &= F_\tau\{F_{t_n}[\Gamma(R_x(t, \tau))]\} \\
 &= \sum_{i=1}^l LVD_{x_i}(f, k) + \sum_{i=1}^{l-1} \sum_{j=i+1}^l LVD_{x_i x_j}(f, k) \\
 &\approx \sum_{i=1}^l A_i^2 \exp(j2\pi a f) \delta(f - f_{0i}) \delta(k - k_i/h)
 \end{aligned} \tag{10}$$

Several studies [29–31] have demonstrated that the LVD algorithm has good noise immunity and estimation performance under Gaussian white noise. However, under impulsive noise conditions, the LVD algorithm fails. The PSIAF and LVD of a single-component LFM signal without noise and with $S\alpha S$ distribution noise are shown in Figure 1. The parameters of the single-component LFM signal used in this simulation are: $A = 1$, $f_0 = 20$ MHz, $k = 40 \times 10^{12}$ Hz/s, $T = 2$ μ s, and the sampling rate $f_s = 256$ MHz. The results show that LVD can accurately detect and estimate the signal parameters without noise. However, under the $S\alpha S$ distribution noise, the PSIAF of the signal is completely corrupted by the noise, leading to failure of the LVD algorithm.

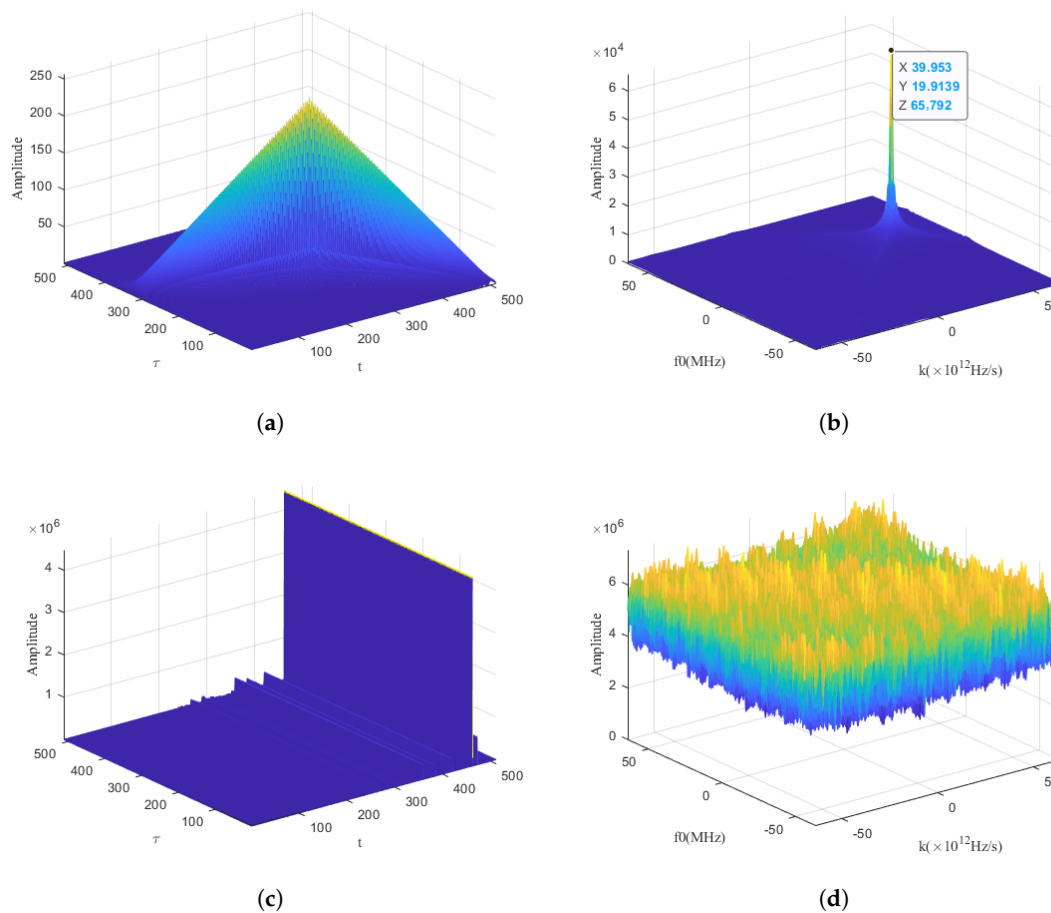


Figure 1. PSIAF and LVD of the LFM signal without noise and with $S\alpha S$ distribution noise. (a) PSIAF (without noise). (b) LVD (without noise). (c) PSIAF (with noise). (d) LVD (with noise).

4. The Improved Lv's Distribution Algorithm

The LVD distribution algorithm is defined in Section 3. It is shown by simulations that LVD cannot achieve parameter estimation of the LFM signal under impulsive noise. To solve this problem, an improved PNAT-LVD algorithm is proposed. The general idea of the algorithm is first to process the LFM signal with impulsive noise using PNAT, then calculate the PSIAF of the processed signal. Next, a scale transformation is performed to decouple the time and time-delay in PNAT-PSIAF. Finally, a two-dimensional Fourier transform is performed to obtain the PNAT-LVD. The estimated values of the parameters are obtained by searching the peak coordinate points. Each step of the algorithm is described in detail as follows.

4.1. Piecewise Nonlinear Amplitude Transform (PNAT)

Traditional nonlinear amplitude transform (NAT) functions have been shown to bear the ability to suppress impulsive noise [20,28,32]. However, the traditional NAT functions, such as the Sigmoid function and compression transform function, have limited noise-suppression ability and are less effective than the FLO methods mentioned before. Although FLO methods can effectively inhibit the impulsive noise, it requires a priori information of the noise. In order to improve the suppression effect on impulsive noise without a priori knowledge, a PNAT function is constructed in the work by [33] to help estimate the multipath delay of the signal in impulsive noise. By combining the truncation function and the PDF of the Cauchy distribution, the PNAT function is defined as Equation (11) [33].

$$PNAT[s(t)] = \begin{cases} s(t), & |s(t)| \leq \eta \\ \frac{2\eta^2 s(t)}{\eta^2 + |s(t)|^2}, & \text{else} \end{cases} \quad (11)$$

where η ($\eta > 0$) is the scale transformation parameter. When $|s(t)| \leq \eta$, the PNAT function directly adopts a linear function, which can retain the valuable information of the signal to the greatest extent. When $|s(t)| > \eta$, the nonlinear part of the PNAT function is obtained by improving the PDF of the Cauchy distribution with decay characteristics. The PNAT can map the pulse with large amplitude to the range of function value uniformly, making the sample more consistent with the Gaussian distribution.

In order to estimate the parameters of the LFM signal in impulsive noise subsequently, the PNAT needs to have two properties: one is that the signal's parameters that need to be estimated cannot change after PNAT; the other is that the signal needs to have finite second-order moments after PNAT. Thus, the following propositions are proposed and proved in this manuscript.

Proposition 1. *The LFM signal changes only in amplitude after PNAT, and the phase information remains unchanged.*

Proof of Proposition 1. Consider a single-component LFM signal, according to Formula (1), the signal can be represented by $x_1(t) = A \exp[j2\pi(f_0 t + \frac{1}{2} k t^2)]$, where A is the amplitude, f_0 is the centroid frequency, and k is the chirp rate. Perform PNAT on $x_1(t)$, we can obtain

When $|x_1(t)| \leq \eta$:

$$PNAT[x_1(t)] = A \exp[j2\pi(f_0 t + \frac{1}{2} k t^2)] \quad (12)$$

When $|x_1(t)| > \eta$:

$$\begin{aligned} PNAT[x_1(t)] &= \frac{2\eta^2 \times A \exp[j2\pi(f_0 t + \frac{1}{2} k t^2)]}{\eta^2 + |A \exp[j2\pi(f_0 t + \frac{1}{2} k t^2)]|^2} \\ &= \frac{2\eta^2 A}{\eta^2 + A^2} \exp[j2\pi(f_0 t + \frac{1}{2} k t^2)] \end{aligned} \quad (13)$$

□

From the above equation, it can be proved that $x_1(t)$ only changes in amplitude, and f_0 and k remain unchanged after the PNAT.

Since the PNAT carries out a linear transformation of the signal when $|s(t)| \leq \eta$, only the suppression ability of impulsive noise in the nonlinear transformation region needs to be considered in Proposition 2.

Proposition 2. *Mutually independent random variables u and v are subject to S&S distribution, and the values of the variables after PNAT are $U = PNAT(u)$ and $V = PNAT(v)$. Then $|E(UV)|$ is bounded in the impulsive noise environment.*

Proof of Proposition 2. Let the joint PDF of u and v be $f_{u,v}(u, v)$, and the scale parameter be η . The nonlinear transformation region is $u, v \in (-\infty, -\eta) \cup (\eta, +\infty)$. From Equation (11), we can then obtain:

$$\begin{aligned}
 |E(UV)| &= \left| E\left(\frac{2\eta^2 u}{\eta^2 + |u|^2} \cdot \frac{2\eta^2 v}{\eta^2 + |v|^2}\right) \right| \\
 &= \left| \int_{-\infty}^{-\eta} \int_{-\infty}^{-\eta} \frac{2\eta^2 u}{\eta^2 + |u|^2} \cdot \frac{2\eta^2 v}{\eta^2 + |v|^2} \cdot f_{u,v}(u, v) dudv \right| \\
 &\quad + \left| \int_{\eta}^{+\infty} \int_{\eta}^{+\infty} \frac{2\eta^2 u}{\eta^2 + |u|^2} \cdot \frac{2\eta^2 v}{\eta^2 + |v|^2} \cdot f_{u,v}(u, v) dudv \right| \tag{14} \\
 &\leq \int_{-\infty}^{-\eta} \int_{-\infty}^{-\eta} \left| \frac{2\eta^2 u}{\eta^2 + |u|^2} \right| \cdot \left| \frac{2\eta^2 v}{\eta^2 + |v|^2} \right| \cdot f_{u,v}(u, v) dudv \\
 &\quad + \int_{\eta}^{+\infty} \int_{\eta}^{+\infty} \left| \frac{2\eta^2 u}{\eta^2 + |u|^2} \right| \cdot \left| \frac{2\eta^2 v}{\eta^2 + |v|^2} \right| \cdot f_{u,v}(u, v) dudv
 \end{aligned}$$

Since $\left| \frac{2\eta^2 u}{\eta^2 + |u|^2} \right| \cdot \left| \frac{2\eta^2 v}{\eta^2 + |v|^2} \right|$ is an even function, the aforementioned equation can be written as:

$$\begin{aligned}
 |E(UV)| &\leq 2 \int_{\eta}^{+\infty} \int_{\eta}^{+\infty} \frac{2\eta^2 u}{\eta^2 + u^2} \cdot \frac{2\eta^2 v}{\eta^2 + v^2} \cdot f_{u,v}(u, v) dudv \\
 &\leq 2 \int_{\eta}^{+\infty} \int_{\eta}^{+\infty} \frac{2\eta^2 u}{\eta^2 + u^2} \cdot \frac{2\eta^2 v}{\eta^2 + v^2} dudv \tag{15} \\
 &\leq 8\eta^4 \int_{\eta}^{+\infty} \frac{u}{\eta^2 + u^2} du \cdot \int_{\eta}^{+\infty} \frac{v}{\eta^2 + v^2} dv
 \end{aligned}$$

When $\eta > 1$, Equation (15) satisfies:

$$|E(UV)| \leq 8\eta^4 \int_{\eta}^{+\infty} \frac{u}{1+u} du \cdot \int_{\eta}^{+\infty} \frac{v}{1+v} dv \tag{16}$$

In the range of $u \in (\eta, +\infty)$, we have $\frac{u}{1+u} \leq \arctan u$, and $\arctan u > 0$, then:

$$\int_{\eta}^{+\infty} \frac{u}{1+u} du \leq \int_{\eta}^{+\infty} \arctan u du \leq \int_0^{+\infty} \arctan u du = \frac{\pi}{2} \tag{17}$$

Similarly, we can obtain $\int_{\eta}^{+\infty} \frac{v}{1+v} dv < \frac{\pi}{2}$, then Equation (12) satisfies:

$$|E(UV)| < 2\eta^4 \pi^2 \tag{18}$$

When $\eta \leq 1$, the Equation (15) satisfies:

$$|E(UV)| \leq 8\eta^4 \left(\int_{\eta}^1 \frac{u}{\eta^2 + u^2} du + \int_1^{+\infty} \frac{u}{\eta^2 + u^2} du \right) \cdot \left(\int_{\eta}^1 \frac{v}{\eta^2 + v^2} dv + \int_1^{+\infty} \frac{v}{\eta^2 + v^2} dv \right) \tag{19}$$

where

$$\int_{\eta}^1 \frac{u}{\eta^2 + u^2} du = \frac{1}{2} \ln \left| \frac{\eta^2 + 1}{2\eta^2} \right| \tag{20}$$

$$\int_1^{+\infty} \frac{u}{\eta^2 + u^2} du = \int_{\frac{1}{\eta}}^{+\infty} \frac{u'}{1 + u'^2} du' < \int_{\frac{1}{\eta}}^{+\infty} \frac{u'}{1 + u'} du' < \int_0^{+\infty} \arctan u' du' = \frac{\pi}{2} \tag{21}$$

Substitute Equations (20) and (21) into Equation (19), we can obtain:

$$|E(UV)| < 8\eta^4 \left(\frac{1}{2} \ln \left| \frac{\eta^2 + 1}{2\eta^2} \right| + \frac{\pi}{2} \right)^2 \tag{22}$$

□

The proposition is proved. Moreover, the value of $|E(UV)| = |E(U^2)|$ is bounded when $u = v$. Therefore, there exist finite second-order moments for random variables that obey the SαS distribution after PNAT.

Since f_0 and k remain unchanged and have finite second-order moments after PNAT, the methods on account of second-order moments can be subsequently used to estimate the parameters. Moreover, the PNAT function can suppress impulsive noise effectively without a priori information about the noise.

4.2. The Improved PNAT-LVD Algorithm

In order to estimate the parameters of the LFM in impulsive noise, an improved PNAT-LVD is proposed. By combining PNAT and PSIAF, a new concept called PNAT-PSIAF is proposed. After performing a scale transformation and a two-dimensional Fourier transform on PNAT-PSIAF, an improved PNAT-LVD algorithm can be obtained. First, the PNAT-PSIAF of the LFM signal is calculated as follows:

$$\begin{aligned} R_x^{PNAT}(t, \tau) &= PNAT \left[x \left(t + \frac{\tau + a}{2} \right) \right] PNAT \left[x^* \left(t - \frac{\tau + a}{2} \right) \right] \\ &= \sum_{i=1}^l R_{x_i}^{PNAT}(t, \tau) + \sum_{i=1}^{l-1} \sum_{j=i+1}^l \left[R_{x_i x_j}^{PNAT}(t, \tau) + R_{x_j x_i}^{PNAT}(t, \tau) \right] \\ &= \sum_{i=1}^l \left(\frac{2\eta^2 A_i}{\eta^2 + A_i^2} \right)^2 \exp[j2\pi f_{0i}(\tau + a) + j2\pi k_i(\tau + a)t] \\ &\quad + \sum_{i=1}^{l-1} \sum_{j=i+1}^l \left[R_{x_i x_j}^{PNAT}(t, \tau) + R_{x_j x_i}^{PNAT}(t, \tau) \right] \end{aligned} \tag{23}$$

For the purpose of decoupling time t and time-delay τ , the scale transformation of Equation (8) is applied to Equation (23), then we obtain

$$\begin{aligned} \Gamma \left[R_x^{PNAT}(t, \tau) \right] &= \sum_{i=1}^l \left(\frac{2\eta^2 A_i}{\eta^2 + A_i^2} \right)^2 \exp \left[j2\pi f_{0i}(\tau + a) + j2\pi \frac{k_i}{h} t_n \right] \\ &\quad + \sum_{i=1}^{l-1} \sum_{j=i+1}^l \left[R_{x_i x_j}^{PNAT}(t_n, \tau) + R_{x_j x_i}^{PNAT}(t_n, \tau) \right] \end{aligned} \tag{24}$$

The expression of PNAT-LVD is then obtained by making a two-dimensional Fourier transformation of t_n and τ based on Equation (24).

$$\begin{aligned} PNAT - LVD_x(f, k) &= F_\tau \left\{ F_{t_n} \left[\Gamma \left(R_x^{PNAT}(t, \tau) \right) \right] \right\} \\ &= \sum_{i=1}^l PNAT - LVD_{x_i}(f, k) + \sum_{i=1}^{l-1} \sum_{j=i+1}^l PNAT - LVD_{x_i x_j}(f, k) \\ &\approx \sum_{i=1}^l \left(\frac{2\eta^2 A_i}{\eta^2 + A_i^2} \right)^2 \exp(j2\pi a f) \delta(f - f_{0i}) \delta(k - k_i/h) \end{aligned} \tag{25}$$

Equation (25) demonstrates that $PNAT - LVD_x(f, k)$ is non-zero only when $f = f_{0i}$ and $k = \frac{k_i}{h}$. By searching the peak of the PNAT-LVD, the coordinate (x_i, y_i) corresponding

to the peak can be obtained. Therefore, the estimation of f_{0i} and k_i based on PNAT-LVD is given by

$$\begin{cases} (x_i, y_i) = \arg \max_{f,k} |PNAT - LVD_x(f, k)| \\ \hat{f}_{0i} = x_i \\ \hat{k}_i = hy_i \end{cases} \quad (26)$$

The scale parameter η in the PNAT function is used to adjust the range of the linear interval to accommodate different kinds of signals and noise. Choosing a suitable η not only helps retain enough helpful information about the signal for the estimation but also suppresses the impulse noise more effectively and improves the PNAT-LVD algorithm’s robustness.

Figures 2 and 3 show the curves of the normalized root-mean-square error (NRMSE) versus the scaling parameter η , which is obtained from 100 Monte Carlo experiments on the LFM signal with different GSNRs and characteristic indexes, respectively. The results show that the NEMSE of the parameters is less than or equal to 0.01 in any case when η is in the range of [1, 7.5). This means that the value of [1, 7.5) ensures the algorithm’s performance. When η equals 1, the algorithm has the best estimation accuracy in all cases. Therefore, $\eta = 1$ is the optimal scale parameter of PNAT and used in subsequent simulations.

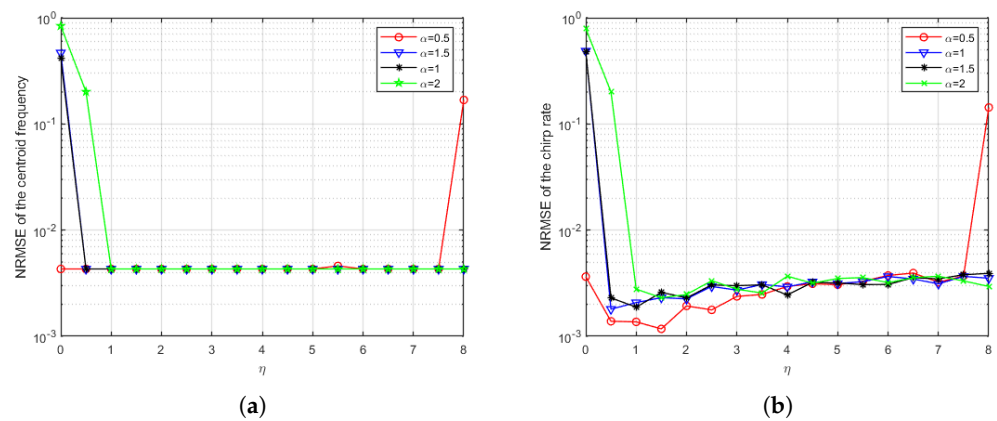


Figure 2. Estimation error of PNAT function for LFM signal with different scaling parameters (GSNR = −4 dB). (a) NRMSE of the centroid frequency. (b) NRMSE of the chirp rate.

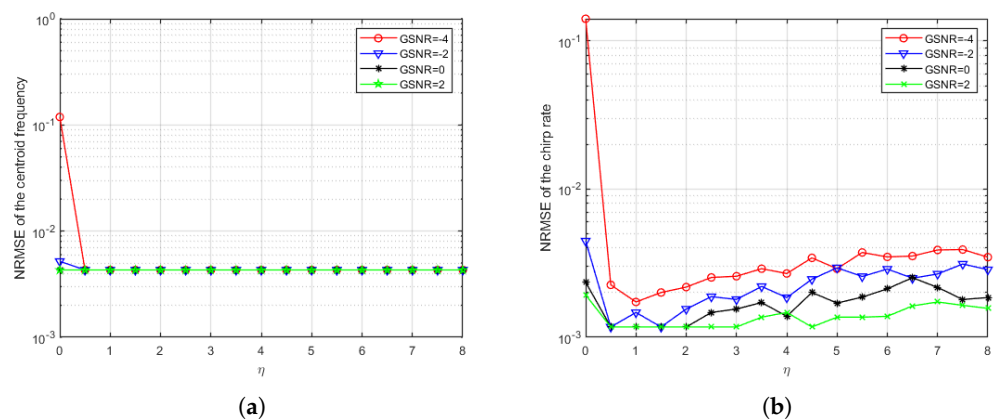


Figure 3. Estimation error of PNAT function for LFM signal with different GSNR ($\alpha = 0.8$). (a) NRMSE of the centroid frequency. (b) NRMSE of the chirp rate.

Figure 4 represents the PNAT-PSIAF and PNAT-LVD of the LFM signal with the $S\alpha S$ distribution noise. The parameters of the signal and noise are the same as that used in Section 3. After applying PNAT, the $S\alpha S$ distribution noise is effectively suppressed,

the PNAT-PSIAF of the signal is no longer completely covered by impulsive noise and the PNAT-LVD exists with a prominent peak accumulated by the LFM signal’s energy.

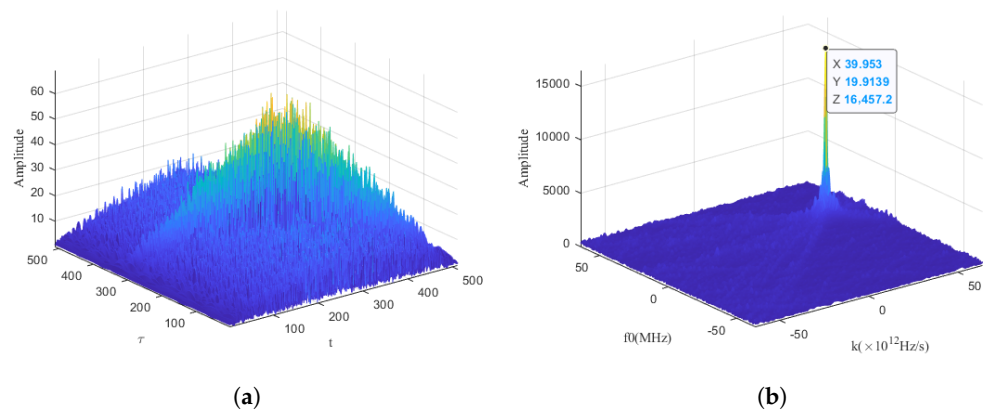


Figure 4. PNAT-PSIAF and PNAT-LVD of the LFM signal with the $S\alpha S$ distribution noise. (a) PNAT-PSIAF. (b) PNAT-LVD.

5. Simulations and Complexity Analysis

5.1. Simulations

We conduct four different types of simulations to assess the performance of the LVD [15], the FLO-LVD [18], the Sigmoid-FRFT [20], and the PNAT-LVD under the $S\alpha S$ distribution noise. The parameters of the single-component LFM signal used in the following simulations are the same as the parameters of the signal component 1 in Table 1. Furthermore, the parameters of the double-component LFM signal used in the following simulations are shown in Table 1. Since the fractional low-order theory has a suppression effect on the $S\alpha S$ distribution noise only when p is in the range of $[0, \frac{\alpha}{2})$, the order of FLO-LVD used in the following simulations is chosen as 0.3.

Table 1. The parameters of the double-component LFM signal.

The Signal Components	The Normalized Amplitude	The Pulse Width (μs)	The Centroid Frequency (MHz)	The Chirp Rate ($\times 10^{12}$ Hz/s)	The Sample Frequency (MHz)
Component 1	1	2	20	40	256
Component 2	1	2	40	−20	256

Simulation 1: A single-component LFM signal’s estimation with different GSNR and α .

Figures 5–7 show the LVD, FLO-LVD, Sigmoid-FRFT, and PNAT-LVD of the LFM signal with $S\alpha S$ distribution noise of different GSNR and α . According to Figure 5, when $GSNR = 0$ dB and $\alpha = 1.5$, all the methods can detect that the signal and the signal’s energy form a distinct peak in a specific domain. The coordinates of the peak correspond to the parameters of the signal. When $GSNR = -6$ dB and $\alpha = 1.5$, Figure 6b,d still show one noticeable peak in the three-dimensional map, while the other methods have failed to detect the LFM signal. When $GSNR = -6$ dB and $\alpha = 0.8$, all methods except for PNAT-LVD fail to detect the signal in Figure 7. Comparing Figure 7d with Figure 6d, PNAT-LVD in Figure 7d suppresses the noise more effectively and estimates the signal parameters more accurately. Since the smaller α is, the stronger the impulsive characteristics of the noise, we can conclude that the PNAT-LVD method performs better than several other methods in a strong impulsive noise environment.

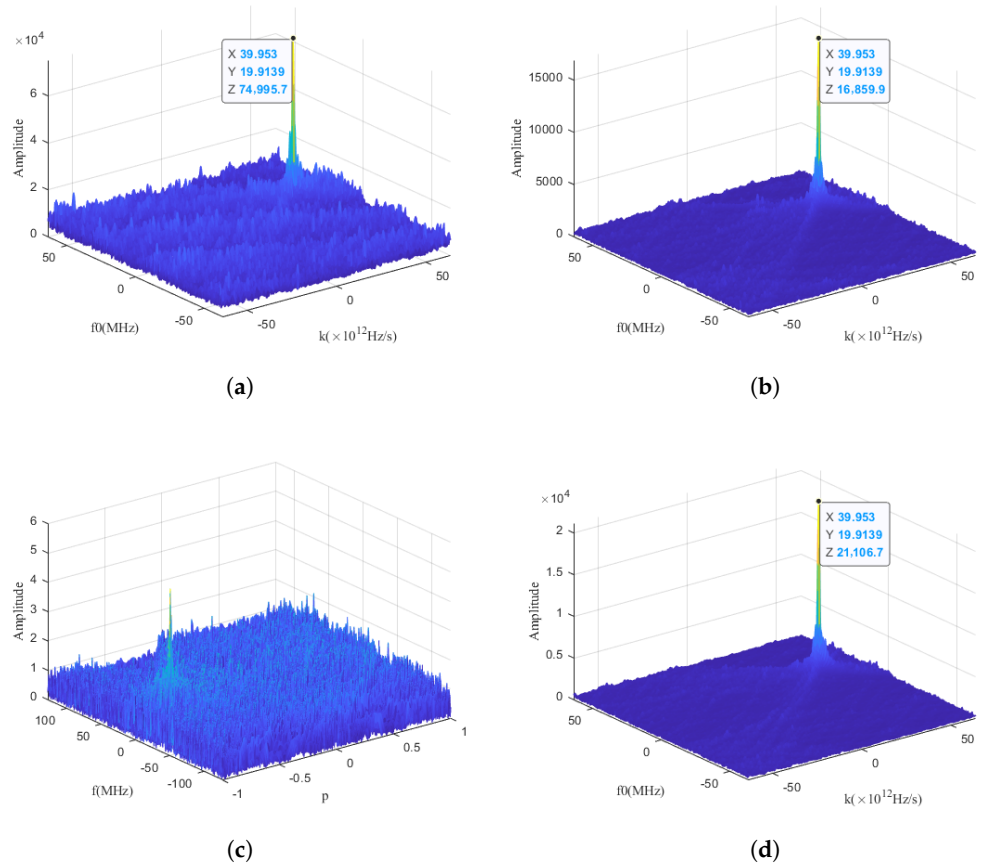


Figure 5. Three-dimensional maps of LVD, FLO-LVD, Sigmoid-FRFT, and PNAT-LVD of the LFM with $S\alpha S$ distribution noise ($GSNR = 0$ dB, $\alpha = 1.5$). (a) LVD. (b) FLO-LVD. (c) Sigmoid-FRFT. (d) PNAT-LVD.

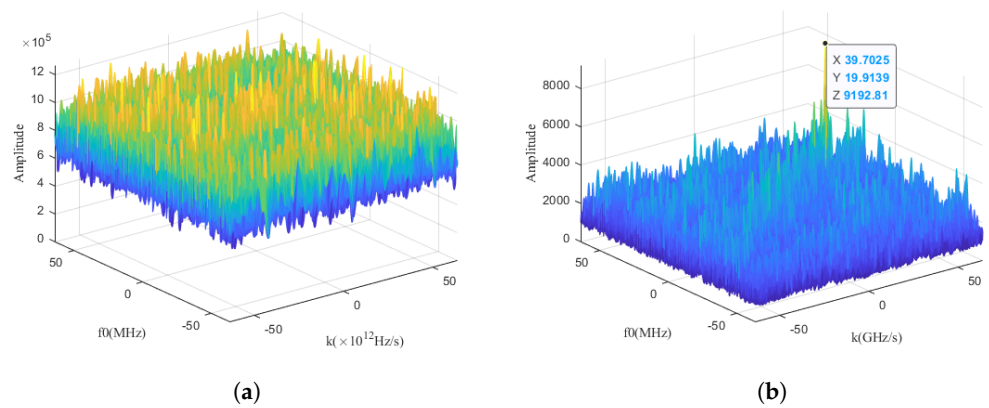


Figure 6. Cont.

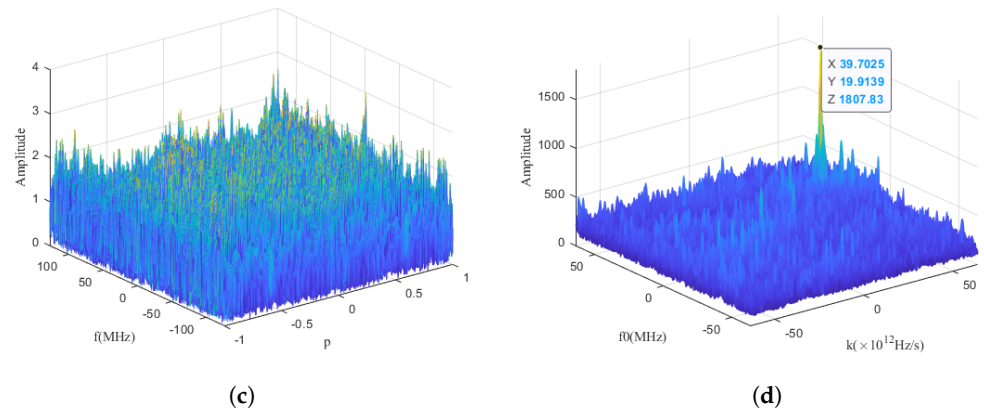


Figure 6. Three-dimensional maps of LVD, FLO-LVD, Sigmoid-FRFT, and PNAT-LVD of the LFM with $S\alpha S$ distribution noise ($GSNR = -6dB, \alpha = 1.5$). (a) LVD. (b) FLO-LVD. (c) Sigmoid-FRFT. (d) PNAT-LVD.

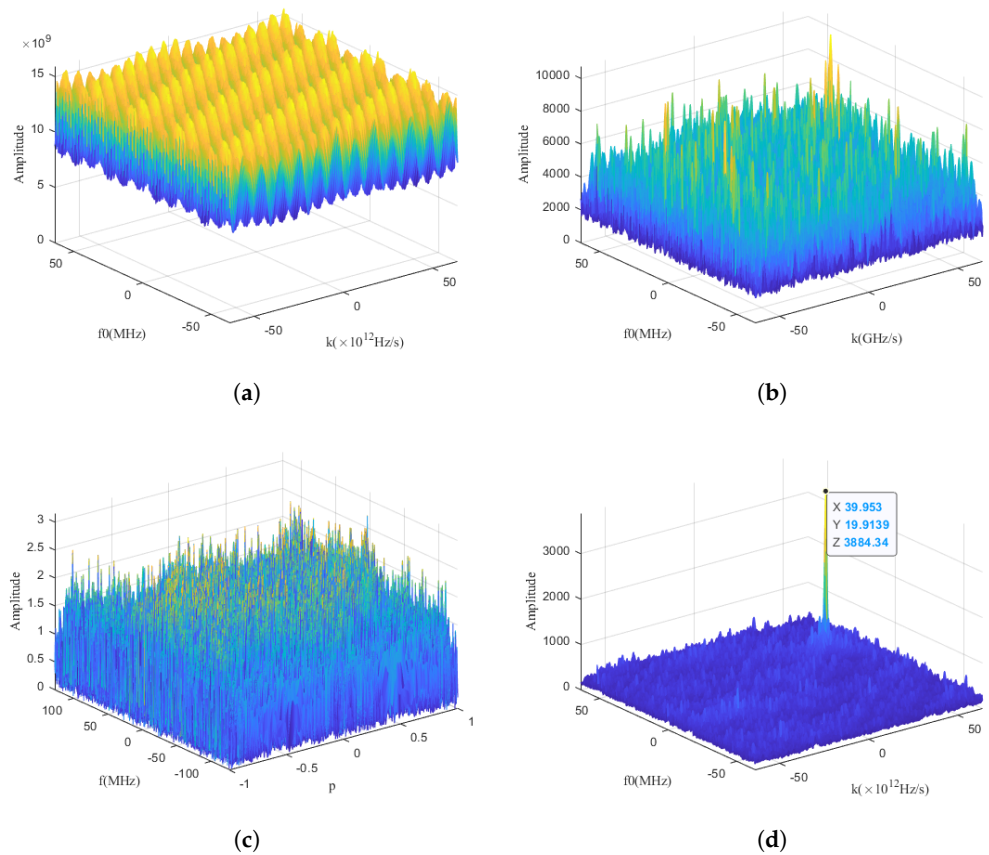


Figure 7. Three-dimensional maps of LVD, FLO-LVD, Sigmoid-FRFT, and PNAT-LVD of the LFM with $S\alpha S$ distribution noise ($GSNR = -6\text{ dB}, \alpha = 0.8$). (a) LVD. (b) FLO-LVD. (c) Sigmoid-FRFT. (d) PNAT-LVD.

Simulation 2: A double-component LFM signal’s estimation with different $GSNR$ and α .

In order to verify the detection capability of the proposed algorithm for the multi-component LFM signal, simulations are performed with the a double-component LFM signal. In total, three backgrounds with different $S\alpha S$ distribution noise are set with the following parameters: (1) $GSNR = 0\text{ dB}, \alpha = 1.5$; (2) $GSNR = -5\text{ dB}, \alpha = 1.5$;

(3) $GSNR = -5$ dB, $\alpha = 0.8$. Figure 8 depicts the detection of the double-component LFM signal using different methods.

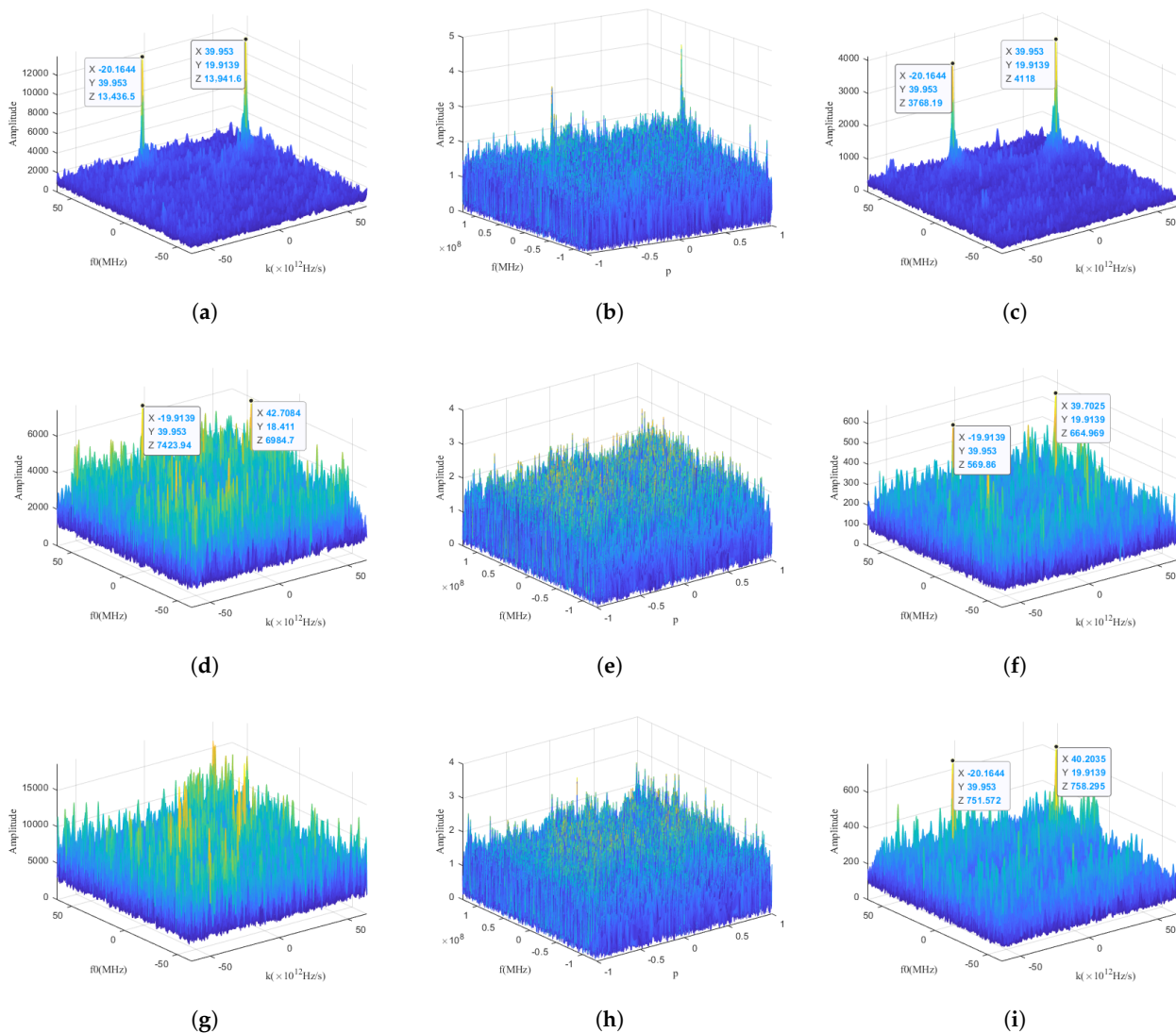


Figure 8. Estimation results of double-component LFM signals using different methods. (a) FLO-LVD ($GSNR = 0$ dB, $\alpha = 1.5$). (b) Sigmoid-FRFT ($GSNR = 0$ dB, $\alpha = 1.5$). (c) PNAT-LVD ($GSNR = 0$ dB, $\alpha = 1.5$). (d) FLO-LVD ($GSNR = -5$ dB, $\alpha = 1.5$). (e) Sigmoid-FRFT ($GSNR = -5$ dB, $\alpha = 1.5$). (f) PNAT-LVD ($GSNR = -5$ dB, $\alpha = 1.5$). (g) FLO-LVD ($GSNR = -5$ dB, $\alpha = 0.8$). (h) Sigmoid-FRFT ($GSNR = -5$ dB, $\alpha = 0.8$). (i) PNAT-LVD ($GSNR = -5$ dB, $\alpha = 0.8$).

The detection results of FLO-LVD, Sigmoid-FRFT, and PNAT-LVD of the double-component LFM signal at $GSNR = 0$ dB and $\alpha = 1.5$ are shown in Figure 8a–c. The energy of the signal components accumulates to form two peaks under the three algorithms, and the signal’s parameters can be accurately estimated by searching for the peak coordinates.

Figure 8d–f indicate the results of FLO-LVD, Sigmoid-FRFT, and PNAT-LVD for the signal at $GSNR = -5$ dB and $\alpha = 1.5$. It can be seen that FLO-LVD and Sigmoid-FRFT have failed at this time, and peaks formed by the energy accumulation of the signal components are covered by the energy of noise. In such situations, the detection and parameter estimation cannot be performed.

To further confirm that the stronger the impulsive characteristics of the noise, the better the suppression effect of PNAT-LVD, Figure 8g–i indicate the results of FLO-LVD, Sigmoid-FRFT, and PNAT-LVD of the signal at $GSNR = -5$ dB and $\alpha = 0.8$. The results show that

only PNAT-LVD is still capable of parameter estimation of the signal. Moreover, comparing Figure 8f with Figure 8i, PNAT-LVD is more effective in suppressing the noise with stronger impulsive characteristics.

Simulation 3: Estimation accuracy with regard to GSNR.

To evaluate the estimation accuracy of several methods for the two parameters of the noisy LFM signal under different GSNR, the NRMSE is used as a criterion to evaluate whether the performance of the method is satisfactory. A total of 100 Monte Carlo experiments are conducted to calculate the variation in NRMSEs of f_0 and k with GSNR, where $\alpha = 1.5$ or $\alpha = 0.8$, and the variation of GSNR is in the range of $[-9 : 10]$ dB with a step size of 1dB. The results are depicted in Figures 9 and 10.

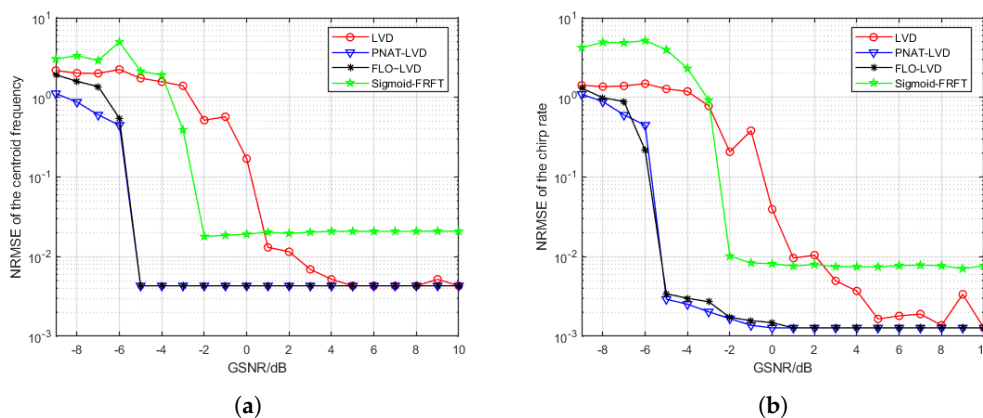


Figure 9. NRMSE of parameters versus GSNR ($\alpha = 1.5$). (a) NRMSE of the centroid frequency. (b) NRMSE of the chirp rate.

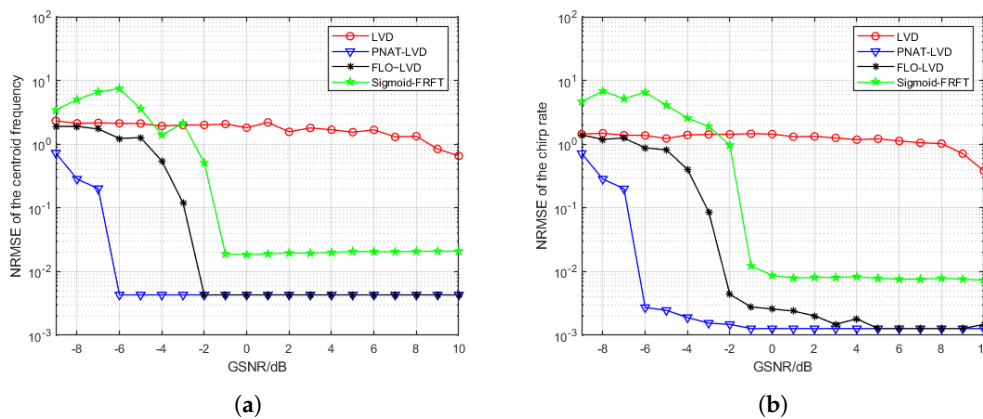


Figure 10. NRMSE of parameters versus GSNR ($\alpha = 0.8$). (a) NRMSE of the centroid frequency. (b) NRMSE of the chirp rate.

Take the NEMSE of the parameter less than 0.02 as the criterion for the algorithm to estimate effectively. Then according to Figures 9 and 10, the estimation accuracy of the centroid frequency using the algorithms concerned with LVD is almost the same when they can achieve effective estimations. However, for the chirp rate, the estimation accuracy of the PNAT-LVD algorithm is much higher than that of the other methods when $\alpha = 0.8$. Table 2 summarizes the minimum GSNR for which different algorithms can achieve effective parameter estimation. As shown in Table 2, PNAT-LVD has the same noise immunity as the FLO-LVD when $\alpha = 1.5$. However, as the α decreases, the performance of all methods degrades except for PNAT-LVD, the noise immunity of PNAT-LVD even improves.

Table 2. The lowest GSNR for which different algorithms can achieve effective parameter estimation.

Characteristic Index	Parameters	LVD	FLO-LVD	Sigmoid-FRFT	PNAT-LVD
$\alpha = 1.5$	f_0	1 dB	-5 dB	-2 dB	-5 dB
	k	1 dB	-5 dB	-2 dB	-5 dB
$\alpha = 0.8$	f_0	-	-2 dB	-1 dB	-6 dB
	k	-	-2 dB	-1 dB	-6 dB

To further compare the estimation performance of various algorithms for the two-component LFM signal, we used different algorithms to perform 100 Monte Carlo experiments for parameter estimation of the double-component LFM signal in the $S\alpha S$ distribution noise with different α . The NRMSE curves of parameters with GSNR are shown in Figures 11 and 12.

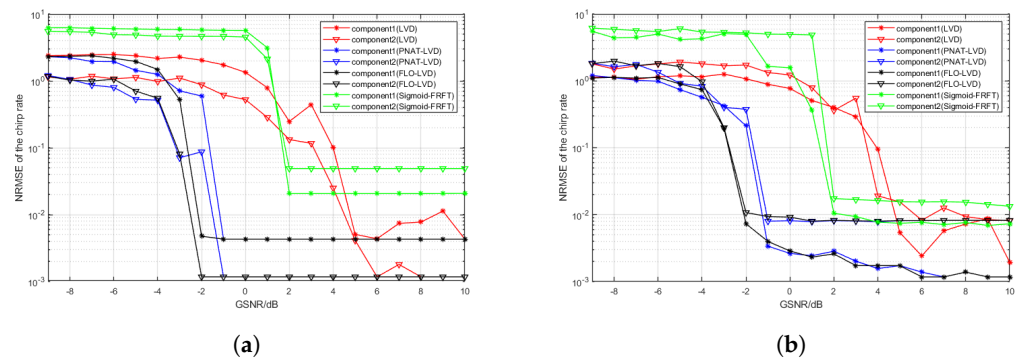


Figure 11. NRMSE of parameters versus GSNR ($\alpha = 1.5$, the double-component LFM signal). (a) NRMSE of the centroid frequency. (b) NRMSE of the chirp rate.

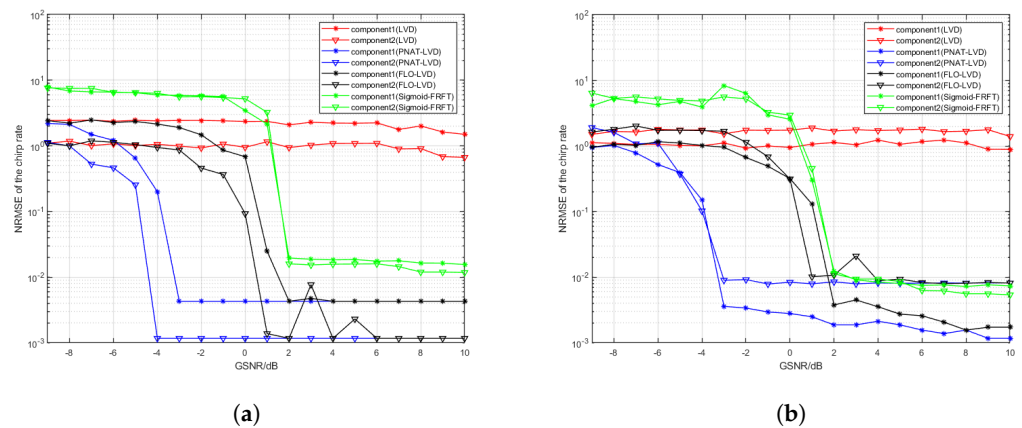


Figure 12. NRMSE of parameters versus GSNR ($\alpha = 0.8$, the double-component LFM signal). (a) NRMSE of the centroid frequency. (b) NRMSE of the chirp rate.

Table 3 summarizes the minimum GSNR of different algorithms that can achieve effective parameter estimation. From the results, when α is equal to 1.5, the noise immunity of the algorithm proposed in this manuscript is slightly worse than that of FLO-LVD. However, when α is equal to 0.8, the noise immunity of PNAT-LVD is much greater than that of the other algorithms, and demonstrates good estimation accuracy. The results once again verify that the stronger the impulsivity of the noise, the more advantageous the PNAT-LVD algorithm is.

Table 3. The lowest GSNR for which different algorithms can achieve effective parameter estimation for the double-component LFM signal.

Characteristic Index	Parameters	The Signal Components	LVD	FLO-LVD	Sigmoid-FRFT	PNAT-LVD
$\alpha = 1.5$	f_0	component 1	5 dB	-2 dB	2 dB	-1 dB
		component 2	6 dB	-2 dB	2 dB	-1 dB
	k	component 1	4 dB	-2 dB	2 dB	-1 dB
		component 2	5 dB	-2 dB	2 dB	-1 dB
$\alpha = 0.8$	f_0	component 1	-	2 dB	2 dB	-3 dB
		component 2	-	1 dB	2 dB	-4 dB
	k	component 1	-	2 dB	2 dB	-3 dB
		component 2	-	1 dB	2 dB	-3 dB

Simulation 4: Estimation accuracy with regard to the characteristic index α of the noise.

Figure 13a,b show the curves of the NRMSE of the centroid frequency and the chirp rate at different characteristic indexes when $GSNR = -2$ dB. The values of characteristic index of the impulsive noise are taken in the range of $[0.5, 2.0]$ with a step size of 0.1, and 100 Monte Carlo experiments are performed at each characteristic index. In Figure 13, the performance of the FLO-LVD rapidly degrades when α is below 0.8. The performance of Sigmoid-FRFT for estimating the centroid frequency degrades when α is less than 0.7, while the performance of Sigmoid-FRFT for estimating the chirp rate degrades when α is less than 0.9. However, the NRMSE of two parameters estimated by PNAT-LVD remains less than 0.01 within the range of the set characteristic index. It can be concluded that the PNAT-LVD algorithm can exhibit excellent estimation performance irrespective of how strong the impulsive characteristics of the noise are. Moreover, the stronger the impulsive characteristics of the noise, the more advantageous PNAT-LVD is compared with the other methods.

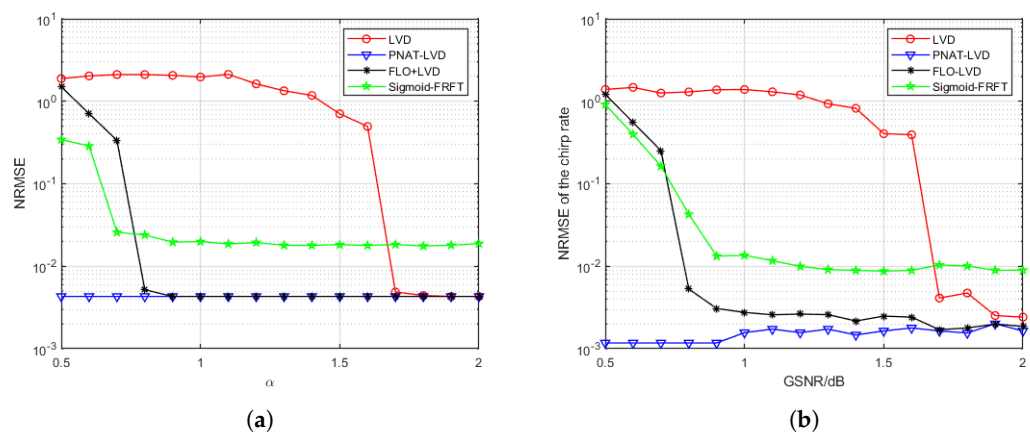


Figure 13. Parameter estimation performance curves of four algorithms for the LFM signal versus characteristic index α . (a) NRMSE of the centroid frequency. (b) NRMSE of the chirp rate.

5.2. Complexity Analysis

Assume the number of time samples is N and the number of searching order required to perform an FRFT is M . The computational cost of LVD and FRFT is in the order of $O(N^2 \log N)$ and $O(MN \log N)$ [19]. The NAT and FLO are mainly for multiplication and division operations, and the computational cost of FLO, Sigmoid transformation and PNAT transformation lies in the order of $O(2N)$, $O(2N)$, and $O(3N)$, respectively. The computational costs of LVD, FLO-LVD, Sigmoid-FRFT and PNAT-LVD are shown in Table 4.

Table 4 shows that the complexity of PNAT-LVD is slightly higher than FLO-LVD and LVD. Since the searching step of the Sigmoid-FRFT used in this manuscript is 0.001, the number of searching order M is 2000. The complexity of PNAT-LVD is much lower than the Sigmoid-FRFT. Therefore, PNAT-LVD improves noise immunity and estimation accuracy compared to the other methods without introducing excessive computational cost.

Table 4. Computational cost.

Algorithm	Computational Cost
LVD	$O(N^2 \log N)$
FLO-LVD	$O(2N + N^2 \log N)$
Sigmoid-FRFT	$O(2N + MN \log N)$
PNAT-LVD	$O(3N + N^2 \log N)$

6. Conclusions

In conclusion, a novel method referred to as PNAT-LVD is proposed for parameter estimation of the LFM signal in impulsive noise. The impulsive noise-suppression ability of the PNAT is analyzed, and the optimal scale parameter when implementing PNAT-LVD is discussed. Results from the simulations verify that the proposed algorithm can effectively suppress the impulsive noise without prior knowledge of the noise for both the single-component and double-component LFM signal. Furthermore, the proposed algorithm exhibits greater precision in estimation accuracy and stronger robustness compared with existing methods.

Author Contributions: Conceptualization, H.W.; methodology, H.W. and Q.Z.; software, H.W. and W.C.; validation, H.W. and J.D.; formal analysis, H.W.; investigation, H.W. and W.C.; resources, J.D.; writing—original draft preparation, H.W.; writing—review and editing, Q.Z. and W.C.; visualization, J.D.; supervision, Q.Z. and X.L.; project administration, X.L. All authors have read and agreed to the published version of the manuscript.

Funding: This research received no external funding.

Conflicts of Interest: The authors declare no conflict of interest.

Abbreviations

The following abbreviations are used in this manuscript:

LFM	Linear frequency modulation
PNAT	Piecewise nonlinear amplitude transform
PSIAF	Parametric symmetric instantaneous autocorrelation function
LVD	Lv's distribution
PNAT-PSIAF	Piecewise nonlinear amplitude transform parametric symmetric instantaneous autocorrelation function
PNAT-LVD	Piecewise nonlinear amplitude transform Lv's distribution
GSNR	Generalized signal-to-noise ratios
LPI	Low probability of intercept
MLE	Maximum likelihood estimator
CRLB	Cramer–Rao Lower bound
FRFT	Fractional Fourier Transform
FLO	Fractional low-order
S α S	symmetric α -stable
PDF	Probability density function

References

1. Li, D.; Zhan, M.; Su, J.; Liu, H.; Zhang, X.; Liao, G. Performances Analysis of Coherently Integrated CPF for LFM Signal under Low SNR and Its Application to Ground Moving Target Imaging. *IEEE Trans. Geosci. Remote Sens.* **2017**, *55*, 6402–6419. [[CrossRef](#)]
2. Martone, M. A multicarrier system based on the fractional Fourier transform for time-frequency-selective channels. *IEEE Trans. Commun.* **2001**, *49*, 1011–1020. [[CrossRef](#)]
3. Misaridis, T.; Jensen, J.A. Use of modulated excitation signals in medical ultrasound. Part I: Basic concepts and expected benefits. *IEEE Trans. Ultrason. Ferroelectr. Freq. Control* **2005**, *52*, 177–191. [[CrossRef](#)]
4. Atkins, P.R.; Collins, T.; Foote, K.G. Transmit-Signal Design and Processing Strategies for Sonar Target Phase Measurement. *IEEE J. Sel. Top. Signal Process.* **2007**, *1*, 91–104. [[CrossRef](#)]
5. Liu, J.; Li, Y.; Li, C.; Gu, C.; Mao, J.F. Accurate Measurement of Human Vital Signs With Linear FMCW Radars Under Proximity Stationary Clutters. *IEEE Trans. Biomed. Circuits Syst.* **2021**, *15*, 1393–1404. [[CrossRef](#)] [[PubMed](#)]
6. Abatzoglou, T.J. Fast Maximum Likelihood Joint Estimation of Frequency and Frequency Rate. *IEEE Trans. Aerosp. Electron. Syst.* **1986**, *AES-22*, 708–715. [[CrossRef](#)]
7. Saha, S.; Kay, S.M. Maximum likelihood parameter estimation of superimposed chirps using Monte Carlo importance sampling. *IEEE Trans. Signal Process.* **2002**, *50*, 224–230. [[CrossRef](#)]
8. Besson, O.; Ghogho, M.; Swami, A. Parameter estimation for random amplitude chirp signals. *IEEE Trans. Signal Process.* **1999**, *47*, 3208–3219. [[CrossRef](#)]
9. Xu, F.; Bao, Q.; Chen, Z.; Pan, S.; Lin, C. Parameter Estimation of Multi-Component LFM Signals Based on STFT+Hough Transform and Fractional Fourier Transform. In Proceedings of the 2018 2nd IEEE Advanced Information Management, Communicates, Electronic and Automation Control Conference (IMCEC), Xi'an, China, 25–27 May 2018; pp. 839–842.
10. Kishore, T.R.; Sidharth, D.S.; Rao, K.D. Analysis of linear and non-linear frequency modulated signals using STFT and hough transform. In Proceedings of the 2015 IEEE International Symposium on Signal Processing and Information Technology (ISSPIT), Abu Dhabi, United Arab Emirates, 7–10 December 2015; pp. 490–494.
11. Gulum, T.O.; Erdogan, A.Y.; Yildirim, T.; Pace, P.E. A parameter extraction technique for FMCW radar signals using Wigner-Hough-Radon transform. In Proceedings of the 2012 IEEE Radar Conference, Atlanta, GA, USA, 7–11 May 2012; pp. 0847–0852.
12. Kalra, M.; Kumar, S.; Das, B. Moving Ground Target Detection with Seismic Signal Using Smooth Pseudo Wigner-Ville Distribution. *IEEE Trans. Instrum. Meas.* **2020**, *69*, 3896–3906. [[CrossRef](#)]
13. Erdogan, A.Y.; Gulum, T.O.; Durak-Ata, L.; Yildirim, T.; Pace, P.E. FMCW Signal Detection and Parameter Extraction by Cross Wigner-Hough Transform. *IEEE Trans. Aerosp. Electron. Syst.* **2017**, *53*, 334–344. [[CrossRef](#)]
14. Moghadasian, S.S. A Fast and Accurate Method for Parameter Estimation of Multi-Component LFM Signals. *IEEE Signal Process. Lett.* **2022**, *29*, 1719–1723. [[CrossRef](#)]
15. Serbes, A. On the Estimation of LFM Signal Parameters: Analytical Formulation. *IEEE Trans. Aerosp. Electron. Syst.* **2018**, *54*, 848–860. [[CrossRef](#)]
16. Aldimashki, O.; Serbes, A. Performance of Chirp Parameter Estimation in the Fractional Fourier Domains and an Algorithm for Fast Chirp-Rate Estimation. *IEEE Trans. Aerosp. Electron. Syst.* **2020**, *56*, 3685–3700. [[CrossRef](#)]
17. Yang, T.; Shao, J.; Chen, Y.; Zhao, Y. Parameter estimation of multi component LFM signals based on nonlinear mode decomposition and FrFT. In Proceedings of the 2018 Tenth International Conference on Advanced Computational Intelligence (ICACI), Xiamen, China, 29–31 March 2018; pp. 204–209.
18. Jin, Y.; Duan, P.; Ji, H. LFM Signal Parameter Estimation Based on LVD in Complex Noise Environment. *J. Electron. Inf. Technol.* **2014**, *36*, 1106–1112.
19. Lv, X.; Bi, G.; Wan, C.; Xing, M. Lv's Distribution: Principle, Implementation, Properties, and Performance. *IEEE Trans. Signal Process.* **2011**, *59*, 3576–3591. [[CrossRef](#)]
20. Li, L.; Qiu, T.S. A Robust Parameter Estimation of LFM Signal Based on Sigmoid Transform Under the Alpha Stable Distribution Noise. *Circuits Syst. Signal Process.* **2019**, *38*, 3170–3186. [[CrossRef](#)]
21. Li, L.; Younan, N.H.; Shi, X. Joint Estimation of Doppler Stretch and Time Delay of Wideband Echoes for LFM Pulse Radar Based on Sigmoid-FRFT Transform under the Impulsive Noise Environment. *Electronics* **2019**, *8*, 121. [[CrossRef](#)]
22. Jin, K.; Lai, T.; Wang, Y.; Li, G.; Zhao, Y. Radar coherent detection for Doppler-ambiguous maneuvering target based on product scaled periodic Lv's distribution. *Signal Process.* **2020**, *174*, 107617. [[CrossRef](#)]
23. Moghadasian, S.S.; Gazor, S. Sparsely Localized Time-Frequency Energy Distributions for Multi-Component LFM Signals. *IEEE Signal Process. Lett.* **2020**, *27*, 6–10. [[CrossRef](#)]
24. Chen, C.; Xu, W.; Dai, J.; Zhou, Y.; Zhang, Y. Performance Analysis of Gini Correlator for Detecting Known Signals in Impulsive Noise. *IEEE Access* **2019**, *7*, 153300–153316. [[CrossRef](#)]
25. Liu, M.; Han, Y.; Chen, Y.; Song, H.; Yang, Z.; Gong, F. Modulation Parameter Estimation of LFM Interference for Direct Sequence Spread Spectrum Communication System in Alpha-Stable Noise. *IEEE Syst. J.* **2021**, *15*, 881–892. [[CrossRef](#)]
26. Wang, J.; Kuruoglu, E.E.; Zhou, T. Alpha-Stable Channel Capacity. *IEEE Commun. Lett.* **2011**, *15*, 1107–1109. [[CrossRef](#)]
27. Jin, Y.; Liu, J. Parameter estimation of frequency hopping signals based on the Robust S-transform algorithms in alpha stable noise environment. *AEU Int. J. Electron. Commun.* **2016**, *70*, 611–616. [[CrossRef](#)]
28. Li, L.; Younan, N.H.; Shi, X. A novel parameter estimation method based on a tuneable sigmoid in alpha-stable distribution noise environments. *Sensors* **2018**, *18*, 3012. [[CrossRef](#)] [[PubMed](#)]

29. Li, L.; Niu, T.; Ji, H.; Han, H.; Liu, Y. Accurate parameter estimation of chirp class signals under low SNR. In Proceedings of the 2016 IEEE International Conference on Signal and Image Processing (ICSIP), Beijing, China, 13–15 August 2016; pp. 412–416.
30. Liu, C.; Luo, Y.; Sun, H.; Xu, Y.; Yu, Z. Application of LV's distribution on the parameter estimation of multicomponent radar emitter signals. In Proceedings of the International Conference on Radar Systems (RADAR 2022), Hybrid Conference, Edinburgh, UK, 24–27 October 2022; pp. 653–656.
31. Zheng, J.; Liu, H.; Liu, Q.H. Parameterized Centroid Frequency-Chirp Rate Distribution for LFM Signal Analysis and Mechanisms of Constant Delay Introduction. *IEEE Trans. Signal Process.* **2017**, *65*, 6435–6447. [[CrossRef](#)]
32. Jin, Y.; Chen, P.; Ji, H. Parameter Estimation of LFM Signals Based on Compress Transform Function in Impulsive Noise. *J. Electron. Inf. Technol.* **2021**, *43*, 277–283.
33. Chen, M.; Xing, H.; Wang, H. Multipath time delay estimation method of LFM signals based on NAT function in impulsive noise. *J. Electron. Meas. Instrum.* **2022**, *36*, 73–81.

Disclaimer/Publisher's Note: The statements, opinions and data contained in all publications are solely those of the individual author(s) and contributor(s) and not of MDPI and/or the editor(s). MDPI and/or the editor(s) disclaim responsibility for any injury to people or property resulting from any ideas, methods, instructions or products referred to in the content.